This is a preprint, the final version is subject to change, of the American Mineralogist (MSA)
Cite as Authors (Year) Title. American Mineralogist, in press.
DOI: https://doi.org/10.2138/am-2019-7043

1 **Revision 1**

2 Formation of saponite by hydrothermal alteration of metal oxides:
3 implication for the rarity of hydrotalcite

4 **Qi Tao [1,2 *], Qingjin Zeng [1,2,3], Manyou Chen [1,2], Hongping He [1,2,3], and Sridhar Komarneni [4]**

5 [1] CAS Key Laboratory of Mineralogy and Metallogeny & Guangdong Provincial Key
6 Laboratory of Mineral Physics and Materials, Guangzhou Institute of Geochemistry, Chinese
7 Academy of Sciences, Guangzhou 510640, P.R. China.

8 [2] Institutions of Earth Science, Chinese Academy of Sciences, Beijing, 100029, P.R. China.

9 [3] University of Chinese Academy of Sciences, Beijing 100049, P.R. China.

10 [4] Department of Ecosystem Science and Management and Materials Research Institute, 204
11 Energy and the Environment Laboratory, The Pennsylvania State University, University
12 Park, PA 16802, USA.

13 * E-mail addresses: taoqi@gig.ac.cn (Q. Tao)

14

This is a preprint, the final version is subject to change, of the American Mineralogist (MSA)
Cite as Authors (Year) Title. American Mineralogist, in press.
DOI: https://doi.org/10.2138/am-2019-7043

ABSTRACT

Conversion of hydrotalcite (Ht) to saponite was observed by hydrothermal alkaline alteration of metal oxides. The conversion was through a pathway of hydration-dissolution-precipitation. It involved several critical steps, including construction of Ht from metal oxides, dissolution of Al^{3+} from Ht, condensation of metasilicate anions with Ht, and finally crystallization of saponite. The condensation was favoured by relatively low Mg/Al ratios of Ht, along with high concentrations of Al^{3+} and silicate oligomers in the environment, resulting in highly crystalline saponite. The latter conversion was greatly accelerated by the isomorphous substitution of Al^{3+} for Si^{4+} in silicate oligomers. The substitution generated the extra negative charge and led to the aforementioned condensation with Ht surface, and thus, promoting the formation of saponite TOT layers. During the process, CO_2 is an indispensable component. Initially intercalated as CO_3^{2-} to form Ht, CO_2 was subsequently eliminated from the solid phase, and saponite formed when the layer charge was reversed. Thus, this study presents a novel formation mechanism of saponite from metal oxides via hydrotalcite, and contributes to a better understanding of the crystallization, chemical stability and transformation of Ht to saponite. The results of the present study are also relevant to evaluating metal availability and carbon cycling on the surface of the Earth.

Keywords: Smectite, Carbonate, Hydrotalcite, Mineral transformation, Saponite

This is a preprint, the final version is subject to change, of the American Mineralogist (MSA)
Cite as Authors (Year) Title. American Mineralogist, in press.
DOI: https://doi.org/10.2138/am-2019-7043

INTRODUCTION

Saponite is a Mg-rich smectite, with a formula of $(Na,Ca)_{0.25}Mg_3(Si,Al)_4O_{10}(OH)_2 \cdot 4H_2O$. It usually forms by weathering of basic or ultrabasic Mg-rich rocks, or through hydrothermal interaction between fluids and igneous materials, and precipitation in alkaline lakes and evaporative basins. (Huang *et al.*, 2013; Setti *et al.*, 2004; Zeyen *et al.*, 2017). Investigations of the processes and mechanisms of saponite formation are of high importance as they may reveal the different processes of its formation and the environments under which it can form (Milesi *et al.*, 2018).

Saponites are increasingly reported to be associated with carbonates, because both kinds of minerals are the main alteration products of basalt under neutral to alkaline conditions (Polyak *et al.*, 2000, Tosca, 2015). Previous researches have revealed the important roles of saponite in the processes of dolomitization or carbonate precipitation and diagenesis, especially under high pH and silicate and/or Mg-rich conditions (*eg.* alkaline lakes and evaporative basins) (Kahle, 1965; Milesi *et al.*, 2018). It can serve as a source of Mg for dolomite formation, as nucleation centers for carbonate crystallization, and as a catalyst to accelerate precipitation of dolomite (Botha and Hughes, 1992; Liu *et al*. 2019; Martín-Pérez *et al*., 2015; Wanas and Sallam, 2016). A very recent study reported that negative charges on the surface of clay minerals can serve as a template and induce the abiotic nucleation of dolomite (Liu *et al*, 2019). The surface charge of saponite is closely related to the occupancy

ratio of Al^{3+} in its tetrahedral and octahedral sheets (Al^{IV}/Al^{VI}) (He *et al.*, 2014; Tao *et al.*, 2018). It can be inferred that the content and distribution of aluminum in saponite structure could play a crucial role in carbonate nucleation and also subsequent interaction of the carbonate with saponite.

Hydrotalcite (Ht) is a naturally occurring but rare anionic mineral on the surface of the Earth. Ht can be regarded as a two-dimensional (2D) carbonate salt, with a formula of $Mg_6Al_2(OH)_{16}CO_3 \cdot 4H_2O$. It contains positively charged brucite-like octahedral layers ($Mg_3Al(OH)_8$), separated by intercalated carbonate anions (CO_3^{2-}), the positive charge being generated by the inequivalent isomorphous substitutions. Due to its CO_3^{2-} intercalated layer structure and exchange property, Ht has a unique feature so as to undergo rapid carbon cycling with the uptake of atmospheric CO_2 under ambient conditions (Ishihara *et al.*, 2013). Natural Ht could be easily formed during the weathering of basalts, or precipitated in saline water sources or alkaline soils associated with clay minerals (*eg.* serpentine), but it was seldom found in large or commercially useful deposits on the Earth (Auerbach *et al.*, 2004). The rare occurrence of Ht deposits is both puzzling and an unsolved issue.

Both experimental and modeling research on the weathering of natural basaltic glass (mainly composed of SiO_2, MgO, Fe_2O_3, Al_2O_3, Na_2O *etc.*) revealed that smectite-like substances can be generated during hydrothermal alteration (Allen *et al.*, 1981; Dehouck *et al.*, 2014; Gooding and Keil, 2013). Hydrotalcite-like compounds

(Htlc) and hydromagnesite ($Mg_5(CO_3)_4(OH)_2 \cdot 4H_2O$) may form during the earlier period of reaction, but subsequently most of them were transformed to clay minerals eventually (Abdelouas *et al.*, 1994). A similar transformation process was also observed in the metal contaminated soils (Jacquat *et al*., 2008; Jacquat *et al*., 2009). In addition, the formation and transformation of the Htlc and saponite were found to be highly dependent on the nature of starting material (such as solid or solution), the type and concentration of cations and pH (Baskaran *et al.*, 2013; Fyfe *et al.*, 1994; Golden *et al.*, 2005; Jacquat *et al*., 2008; Jacquat *et al*., 2009; Schutz and Biloen, 1987; Yun, 1995).

The formation of carbonates and Mg-smectites requires very similar alkaline environments. We have therefore chosen mixed metal oxides as a basalt analogue, and assessed their reactivity and transformation under hydrothermal conditions. The mechanisms of the hydration of metal oxides to form Ht, and its further conversion to saponite were determined using a variety of characterization techniques such as XRD, ^{27}Al and ^{29}Si NMR, TEM *etc.* The new findings of this research contribute to a better understanding of the crystallization, chemical stability and transformation of Ht to saponite. This study also has implications for metal availability and carbon cycling on the surface of the Earth.

SAMPLES AND METHODS

Mineral preparation and transformation

Ht with Mg/Al molar ratios of 2, 4, 6 were synthesized using a co-precipitation method (Tao *et al.*, 2011). In the present instance, 0.1 mol $Al(NO_3)_3$ and suitable amount of $Mg(NO_3)_2$ were dissolved in 300 mL ultrapure water. After stirring (300 r/min), the formed mixture was dropped into a 300 mL ultrapure water using an autosampler at a fixed ratio (15 mL/min). Meanwhile, sodium hydroxide solution (5.0 mol/L) was added intermittently to maintain the pH of the mixed solution at 10.00 (± 0.05) by an automatic pH control equipment (Chromar, PR China). The above mixture was stirred for 2 h and then aged in an 80°C water bath for 12 h. The obtained samples were denoted as Ht-n where n denotes the molar Mg/Al ratio (2, 4, 6), respectively. The mixed metal oxides (MMO) were obtained by calcination of Ht at 500°C for 6 h. The calcined products were denoted as MMO-n, respectively.

Mineral transformation experiments were conducted in an alkaline solution containing 33.8 mmol of $Na_2SiO_3 \cdot 9H_2O$ and 90.0 mmol of NaOH dissolved in 120 mL ultrapure water. A suitable amount of $NaHCO_3$ (*eg.* 66.2 mmol) was added to the above solution as a pH buffer. With stirring, 2.47 g MMO (containing 30.0 mmol Mg^{2+} and 15.7 mmol Al^{3+} for MMO-2, as an example) was put into the above freshly prepared alkaline solution. After thoroughly stirring, the mixture was transferred to a Teflon-lined autoclave (with a capacity of 200 ml) and hydrothermally treated at 160°C

for different times (t = 0, 1, 4, 10, 15, 30, and 60 days). In all the reaction procedures, the pH values were over 14.0 as calculated from the added alkali. The obtained gel-like mixtures were washed with ultrapure water 6 times by centrifuge-washing until the supernatant reached neutral pH, and then the gel was dried at 80°C followed by grinding prior to characterization. The obtained products were marked as MMO-n-t, where 'n' represents Mg/Al ratio, and 't' represents treatment time. Among them, MMO-n-0 represents the samples produced by the stirring of MMO-n and alkaline solution for 5 min (without undergoing hydrothermal treatment).

The effect of SiO_3^{2-} on the phase and composition of the final products was investigated by adding the anion at a concentration of 0.5, 1.0, and 4.0 times that of the anion exchange capacity (AEC) of Ht derived from the chemical formula of Ht-n. The products are labeled as MMO-n-t-x where x (0.5, 1.0, 4.0) denotes the AEC multiplier.

Transformation of Ht to saponite was carried out by the following process: 74.0 mmol $Na_2SiO_3 \cdot 9H_2O$ was dissolved in 120 mL ultrapure water. After stirring, the solution was transferred to a Teflon-lined autoclave, together with a suitable amount of Ht of 200 mesh (keeping Mg= 65.0 mmol, and Mg/Al=2, 4, and 6, respectively). After stirring for another half an hour, the autoclave was sealed and heated at 160°C for 4 days. The obtained gel-like mixtures were treated as described above and marked as Ht-n-4.

Analysis methodology

X-ray diffraction (XRD). XRD patterns were collected between 1° and 65°(2θ) at a scanning rate of 1° min^{-1} on a Bruker D8 Advance diffractometer with Ni-filtered CuKα radiation (λ=0.154 nm, 40 kV and 40 mA).

X-ray fluorescence spectroscopy (XRF). Elemental analysis was conducted on a Rigaku RIX 2000 X-ray fluorescence spectrometer. Loss-on-ignition (L.O.I.) was obtained by mass loss of the sample ignited in a furnace at 900°C for 2 h and subsequently cooled to *r.t.* in a desiccator to minimize moisture absorption. About 500 mg of calcined sample and 4 g $Li_2B_4O_7$ were mixed homogeneously, and then digested in a Pt-Au alloy crucible at 1150°C in a high-frequency furnace. The calibration line for Si/Al ratio used in quantification was produced by bivariate regression of the Si/Al data measured for 36 reference materials encompassing a wide range of silicate compositions, and analytical uncertainties were mostly between 1 and 5% (He *et al*., 2014).

Solid state magic-angle-spinning nuclear magnetic resonance spectroscopy (MAS NMR). Both ^{27}Al and ^{29}Si MAS NMR experiments were performed on a Bruker AVANCE III 600 spectrometer at resonance frequencies of 156.4 and 119.2 MHz, respectively. ^{29}Si MAS NMR spectra with high-power proton decoupling were recorded on a 4mm probe with a spinning rate of 12 kHz, a π/4 pulse length of 2.6 μs, and a recycle delay of 80 s. The chemical shifts of ^{29}Si were referenced to

tetramethylsilane (TMS). A 4 mm HX double-resonance MAS probe was used to measure ^{27}Al MAS NMR at a sample spinning rate of 14 kHz. The spectra were recorded by a small-flip angle technique with a pulse length of 0.5 μs ($< \pi/12$) and a 1s recycle delay. The chemical shifts of ^{27}Al were referenced to 1 mol L^{-1} aqueous $Al(NO_3)_3$.

Transmission electron microscopy (TEM). TEM images, X-ray energy-dispersive spectroscopy (EDS) analyses, and selected-area electron diffraction (SAED) patterns were obtained by a FEI Talos F200S machine at 200 kV, equipped with Super X X-ray spectroscopy. Specimens were prepared by dispersing the samples in ethanol and ultrasonically treating them for 5 min. A drop of the resultant suspension was placed on a porous carbon film supported by a copper grid, after which the ethanol was evaporated.

RESULTS AND DISCUSSION

Phase transformation during hydrothermal reaction

MMO was mainly composed of a poorly crystallized periclase phase (▽, MgO, PDF#: 075-1525) as shown by XRD patterns (Figs. 1Aa, 1Ba and 1Ca) (Tao *et al.*, 2010). After mixing with alkaline solution, it was rapidly hydrated and transformed to Ht structure (✧, PDF#: 41-1428). For the MMO-n-0 samples, a series of reflections were recorded at *ca.* 11.4°, 22.9°, 35.1°, 60.7° and 62.1° (2θ) (Fig. 1A), corresponding

to a typical and well-ordered layered structure of Ht with d_{003} values in the range of 0.763–0.787 nm. Since the d_{003} values of the CO_3^{2-} and NO_3^- intercalated Ht are usually occur at 0.760–0.780 nm and 0.813–0.894 nm, respectively (Duan and Evans, 2006), it would appear that CO_3^{2-} dominated the interlayer space of the Ht. The CO_2 was readily adsorbed from air atmosphere to be fixed in the interlayer of Ht as CO_3^{2-}, even with the presence of nitrate in the starting solution. As no other carbonate phase was detected by XRD (Fig. 1A), CO_3^{2-} was presumably expelled from the solids and escaped into the aqueous surroundings following conversion of Ht to saponite.

For the MMO-4-t series of products, the formed Ht almost vanished after 10 days of hydrothermal treatment, judging by its characteristic XRD reflections. Meanwhile, a new series of broad and weak XRD reflections emerged at *ca.* 6.5°, 19.6°, 26.7°, 38.7°, 62.5° (2θ) *etc.*, which are attributed to the reflections of newly formed smectites (Fig. 1B). The reflection at *ca.* 6.5° with a d value of 1.290 nm, is a typical d_{001} value of Na^+ intercalated smectite (Tao *et al.*, 2016). This value increased to ca. 1.66 nm after the sample was saturated by ethylene glycol (Fig. S1.). Furthermore, the diagnostic reflection at *ca.* 62.5° was ascribed to (060) reflection with a d value of 0.154 nm, which verified that it is a trioctahedral smectite, *i.e.*, saponite (♦, PDF#: 30-0789). All the reflections of Ht gradually decreased in intensity but vanished at 10 days of reaction, and meanwhile the (001) reflections of saponite continually intensified during 60 days of hydrothermal treatment (Fig. 1B). Throughout the conversion of Ht to saponite,

another series of weak but sharp reflections at *ca.* 14.0°, 19.1°, 24.4° and 27.8° also occurred, which are attributed to natrodavyne (▼, $NaAlSiO_4$, pdf#: 15-0469). The appearance of natrodavyne represents a Si and Al-rich alkaline environment, implying that Si and Al were in excess during smectite formation in this case.

The MMO-2-t series of products were formed through a very similar process, except that the crystallinity of saponite reached maximum by 10 days, and the content of natrodavyne was very much higher compared with those of MMO-4-t series. By increasing the Mg/Al molar ratio to 6 in the precursor material, a decrease in the crystallinity of both the intermediate Ht and the final saponite occurred as revealed by the XRD results of MMO-6-t series of samples. The appearance of brucite phase at the beginning of hydrothermal treatment suggested that the Mg^{2+} was in excess and hence transformed to brucite at the initial stage.

The disappearance of Ht with the concomitant increase in saponite indicated that Ht was an unstable phase when silicate anions coexisted in the alkaline solutions. The reactions would proceed further with silicate anions and form smectite.

Mg/Al molar ratio on Ht transformation and saponite crystallization

The chemical stability of minerals is sensitive to the variation of geological conditions. Therefore, to well understand their formation process, it is a priority to constrain the limits and controls at their initial precipitation and during their

209 crystallization (Tosca *et al.*, 2008; Tosca, 2015). By analyzing the changes of mineral
210 species and elemental composition of samples before and after the reaction, the detailed
211 occurrence state and the behaviors of the cations can be revealed.

212 Calculations of the XRF analyses showed that the Mg/Al molar ratios were 2.46,
213 4.83 and 7.55 for MMO-2-0, MMO-4-0 and MMO-6-0, respectively (Table 1). These
214 values slightly decreased compared to the respective starting materials during
215 hydrothermal treatment, and the larger the starting material Mg/Al ratio, the greater
216 was the extent of the decrease after treatment. Previous studies revealed that
217 (Si+Al)/Mg = 4:3 was an optimized ratio to form well-ordered saponites with Si/Al
218 ratios in the range of 5.43–7.89 (He *et al.*, 2014; Tao *et al.*, 2016). Based on these
219 values, the optimized Mg/Al ratio to form saponite are calculated as *ca.* 6.67–9.09 in
220 this case. This implied that although Mg^{2+} was relatively insufficient as in MMO-2-0
221 and MMO-4-0, it would still be partly dissolved from MMOs during their hydration
222 and transformation processes.

223 On the other hand, the Si/Al ratios of the products gradually increased with the
224 extension of reaction time. For the products at 15 days, the Si/Al values were
225 approximately equivalent to the respective Mg/Al and were in the range of the ratio for
226 the ideal saponite formation. This is the reason why these saponites showed much
227 higher crystallinity (Figs. 1A-h and 1B-h).

228 Hydration of MMO to form Ht structure was a very fast process, being largely

229 completed even before the hydrothermal treatment (MMO-n-0). The products usually
230 contained some residual periclase or brucite, the amount of which depended on the
231 concentrations of Mg^{2+}. When Mg/Al≤4, the products showed some residual periclase
232 (Figs. 1A and B). However, when the Mg/Al = 6, the periclase completely converted to
233 brucite because of the presence of excess Mg^{2+} (Fig. 1C). As the reaction time
234 prolonged, the reflections of the intermediate hydrotalcite phase and brucite gradually
235 weakened and finally disappeared, while the (001) reflection of saponite continued to
236 increase, indicative of increased stacking order along the c-axis. Meanwhile, the (02,11)
237 reflection of saponite gradually intensified with time, indicating that the crystallinity of
238 saponite in the a-b direction also gradually increased. The larger the Mg/Al ratio, the
239 lower was the crystallization of saponite. After a 15-day reaction period, all saponite
240 products reached their highest crystallinities and remained at this level even with
241 prolonged further hydrothermal treatment.

242 These findings are consistent with the observed increase in the dehydroxylation
243 temperatures and the related mass losses of both Ht and saponite as indicated by the
244 TG-DTG curves (Fig. S2). Ht products with Mg/Al = 6 showed the lowest
245 dehydroxylation temperature (390°C), followed by the samples with Mg/Al = 4 (427°C)
246 and 2 (430°C) (Fig. S2). This indicated that Ht formed with Mg/Al = 4 was the most
247 stable. As the Mg/Al ratio increased, the mass losses of Ht through dehydroxylation
248 increased, while the temperature of dehydroxylation for saponite gradually decreased

(780°C). The dehydration mass loss of saponite was the least for the sample with Mg/Al = 4, and the most for the sample with Mg/Al = 6. The dehydroxylation temperatures of hydrotalcite and saponite for all the three series of samples were ca. 560°C and 780°C, respectively. This result indicated that the crystallinity of the two phases was similar under these conditions, and they did not change with the concentrations of cations initially used. Based upon these results, we may therefore conclude that a low Mg/Al ratio or a high Al concentration is conducive to saponite crystallization.

Influence of cation occupancy and migration of cations on the conversion of Ht to saponite

The occupancy of the cations involved in the transformation of Ht to saponite was further disclosed by solid-state ^{27}Al and ^{29}Si MAS NMR spectroscopy (Fig. 2). The ^{27}Al NMR spectra of saponite generally show signals at 0–20 ppm for octahedral (Al^{VI}) and 50–75 ppm for tetrahedral coordinated Al (Al^{IV}) respectively (Bisio *et al.*, 2008). ^{29}Si NMR spectrum of saponite is usually represented by Q^x(yAl) (x = 1–3, and y = 0–4, where Q^x represents the degree of polymerization of Si in the tetrahedral sheet (Smith *et al.*, 1983), x represents the Si coordination number, and y represents the number of Al^{IV} around Si (Lipsicas *et al.*, 1984).

All the MMO samples show a ^{27}Al signals located at about 11 ppm, attributable to the Al^{VI} in periclase (Fig. 2a-c). These signals became weaker and broader after 4 days

of treatment, due to the conversion of periclase to Ht. They further decreased in intensity and became broader with increasing reaction time, and meanwhile a new signal appeared and gradually intensified at 68 ppm, corresponding to Al^{IV} of newly formed saponite (Fig. 2 (left)). The intensity ratio of Al^{IV}/Al^{VI} signals increased with the prolonged hydrothermal treatment, which indicates the migration of Al from the octahedral to the tetrahedral sites of saponite during the transformation of Ht and crystallization of saponite from Ht (He *et al.*, 2014). The other Al^{IV} signal at *ca.* 62 ppm (Fig. 2 (left)) was ascribed to Al^{IV} in natrodavyne. The appearance of natrodavyne represented a silicon and aluminum enriched environment. Its intensity became significantly weaker as in the case of MMO with higher Mg/Al ratio, which implies that the presence of natrodavyne is dependent on the availability of Al^{3+} in the dissolved form from the solids, indicating that Al^{3+} was partly dissolved from the reactants during the conversion to saponite.

The ^{29}Si NMR spectra of the products mainly exhibited four kinds of Si signals (Fig. 2 (right)). The resonances at –85 ppm and –94 ppm were attributed to Q^2Si(0Al) and Q^3Si(0Al) environments, respectively in the saponite tetrahedral sheet (Vogels *et al.*, 2005). The Q^2 signal was caused partly by the broken bonds at the lateral surface of saponite (He *et al.*, 2014; Tao *et al.*, 2016). Signal at –89 ppm, ascribed to the Q^3Si (1Al) environment of saponite, overlapped with the Si-O-$(Al)_4$ of natrodavyne (Shao and Pinnavaia, 2010). Furthermore, a shoulder signal at –81 ppm in the spectrum of

MMO-6-4 attributed to incompletely condensed SiO_3^{2-} (Fig. 2f (right)). The appearance of this shoulder indicated the beginning of the condensations between SiO_3^{2-} at the surface, as well as in the interlayer space, which apparently led to a rather disordered Si coordination environment. The well resolved resonances in the ^{29}Si NMR spectra at –85, –89 and –94 ppm revealed the generation of saponite with high crystallinity, but accompanied by natrodavyne in MMO-2 and 4 series of products (Figs. 2d-f (right)).

Concentration of SiO_3^{2-} on the conversion of Ht to saponite

Prior research indicated that Si/Al ratio in the tetrahedral sheet has a decisive effect on the formation and crystallinity of saponites (He *et al.*, 2014; Tao *et al.*, 2016; Vogels *et al.*, 2005). To disclose such an influence on the transformation of MMOs, MMO-4 was reacted with different concentrations of SiO_3^{2-}, because its Mg/Al ratio was suitable for both Ht and saponite formation as discussed above.

When the relatively lower SiO_3^{2-} concentrations (≤ 1.0AEC) were applied, the products were dominated by well crystallized Ht along with some brucite, the latter formed by periclase hydration as shown by XRD patterns (Fig. 3). The d_{003}= 0.769 nm and the stretching absorption at 1395 cm^{-1} in FTIR spectra confirmed that CO_3^{2-} dominated the interlayer space of Ht (Fig. S3), and possibly partially mixed with SiO_3^{2-} and/or its oligomeric anions (Baskaran *et al.*, 2013; Fyfe *et al.*, 1994; Yun, 1995). A very weak hump at *ca.* 70 ppm in ^{27}Al NMR spectrum was attributed to the partial substitution of Al^{3+} for Si^{4+} in silicate oligomeric anions (Figs. 4 (left)), which

confirmed the dissolution of Al^{3+} from Ht during the conversions. In these cases, the reaction time had little or no contribution to the final phases.

When the SiO_3^{2-} concentration exceeded 4.0AEC, the main product was saponite (d_{001} = 1.260 – 1.330 nm, and d_{060} = 0.154 nm) with a small amount of Ht. The reflections of Ht phase and the absorption of CO_3^{2-} stretching dramatically decreased with time and finally vanished (Fig. 3 and Fig. S3). Meanwhile, the XRD reflections of saponite became sharper (Fig. 3) and the FTIR absorptions corresponding to the polymerized silicate oligomer anions intensified in the wavenumber region of 999–1100 cm^{-1} (Fig. S3). Besides, the Mg-OH stretching at 3690 cm^{-1} was reduced in intensity, implying that the number of free Mg-OH groups at the brucite surface decreased, as a result of the condensation with the silicate oligomer anions. A new weak but well resolved band appeared at 817 cm^{-1}, which is ascribable to Si-O-Al linked to the octahedral sheet via an oxygen bridge (Farmer, 1974). The appearance of this absorption marked the beginning of the transformation of brucite-like layers (including brucite layers and Ht layers) towards saponite. This can be verified by the intensified resonance of Al^{IV} and the weakened Al^{VI} resonance in ^{27}Al NMR spectra (Figs. 4 (left)). Further increasing the concentration of SiO_3^{2-} led to the disappearance of brucite, and generation of some natrodavyne and increase in the crystallinity of saponite (Fig. 3). Further evidence was provided by the increase in intensity of Mg-OH stretching and Si-O-Si stretching absorptions (Figs. S3g, h), and intensity ratio of Q^3/Q^2

329 as shown by the ^{29}Si NMR spectra (Fig. 4 (right)).

330 As already mentioned, SiO_3^{2-} can be incorporated in solid during hydrothermal
331 treatment through two pathways that are separated by a concentration of 4AEC. Below
332 this concentration, it would be adsorbed on the surface of Ht, as well as enter its
333 interlayer space to balance the layer charge. When the SiO_3^{2-} was sufficiently high (≥
334 4AEC), the highly condensed silicate oligomeric anions would form with partial
335 substitution of Al^{3+} for Si^{4+}. They would rapidly be connected with Ht and brucite
336 octahedral sheet (positively charged), and thereby further crystallizing to form saponite.
337 On the other hand, it would therefore appear that octahedrally coordinated Al^{3+} can
338 migrate to tetrahedral sites during saponite formation.

339 **TEM observation on morphological characteristics of transformation products**

340 TEM images, along with EDS results and SEAD patterns can provide the direct
341 information on products' morphology, composition and phase. MMO with Mg/Al=2
342 showed the highest conversion rate to form saponite. The TEM images exhibited
343 mainly thick flaky and several long columnar morphologies, corresponding to saponite
344 and natrodavyne, respectively of the sample reacted for 1 day (Fig. 5). The edge of the
345 thick flaky particle displayed a curled ribbon-like morphology, and the surface of the
346 central region was very rough. According to chemical formula and XRF results, the
347 composition of the hydrotalcite/brucite, natrodavyne, and saponite should theoretically
348 be limited to regions of $1.19 \leq Mg/(Si+Al) \leq 2.38$, $Mg/(Si+Al) \approx 0$, and $Mg/(Si+Al) =$

349 0.75, respectively (Table 1). The EDS results indicated that the Mg/(Si+Al) atomic
350 ratios were 0.00 and 0.53 for the selected areas of the long columnar mineral (Fig. 5, P1)
351 and the flaky particles (Fig. 5, P2), respectively. These values are basically located in
352 their theoretical composition regions.

353 The particles of saponite that formed after 15 days of reaction are thin and curled,
354 typical of this mineral species (He *et al.*, 2014; Tao *et al.*, 2018). No obvious
355 natrodavyne or Ht phase was observed after 15 days of reaction. EDS results showed
356 that the Mg/(Si+Al) = 0.65 (Fig. S4, P), suggesting the composition of saponite trended
357 towards ideal composition while its crystallinity increased continuously.

358 Increasing the Mg/Al ratio to 4 appears to slightly slow down the conversion rate
359 of the intermediate products. Therefore, it could still be recognized in the form of Ht in
360 the residues with a hexagonal sheet morphology as in the case of original Ht (Fig. S5a).
361 These residues were surrounded by the newly formed saponite with curled sheets. By
362 extending the reaction time to 2 days, the products displayed a ribbon-like curled flake
363 predominantly, indicating that the conversion was promoted remarkably (Fig. S5b).

364 MMO-6 series of samples have the lowest conversion rate compared with those of
365 the other two series of samples, which helps to obtain more details of the transformation
366 process. MMO-6-2 sample appeared as flaky particles with a hexagonal outline,
367 partially retaining the features of Ht and brucite (Fig. 6). The curled lamellar
368 morphology of saponite was clearly displayed at the edges of mineral aggregates and

single particles. A representative single particle is shown in Fig. 6b. Three different morphologies were demonstrated from the inside to the outside of the particle, including a flat Ht or brucite sheet with rough surface, a broken inclusion-like transition phase, and a curled flake of saponite.

The selected area electron diffraction analysis (SAED) was carried out to verify this observation (Fig. 6, P1-P3). The central region in the diffraction was attributed to the single crystal phase of hydrotalcite/brucite (Fig. 6, P1). The maximum d-value corresponding to the spot distance to the deflection center coincided with the d_{113} value of the hydrotalcite. The transition region between the central and the edge basically exhibited a mixture of Ht and saponite (Fig. 6, P2) with hydrotalcite as a major phase and saponite as a very minor one. It might imply the beginning of the transformation of Ht to saponite. The edge region showed diffraction rings attributed to the polycrystalline phases, including a phase with a d-value = 0.221 nm, ascribed to a combination of the (202) plane of saponite, and the (113) plane of Ht (Fig. 6 P3). These SAED results are consistent with the TEM morphology observations.

The MMO-6-4 sample has an egg-like core-shell morphology can be observed for (Fig. 7). According to XRF results, the composition of the hydrotalcite/brucite and saponite should theoretically be located in the region of $3.66 \leq Mg/(Si+Al) \leq 7.32$ and $Mg/(Si+Al) = 0.75$, respectively (Table 1). The Mg/(Si+Al) of the core and shell sites were calculated as 6.15 and 0.61, respectively by EDS data. These values confirmed

that the phases were hydrotalcite and saponite, respectively. Moreover, the SEAD patterns displayed d=0.147, and 0.221 nm diffraction spots, which also support the presence of the above phases.

The Mg/(Si+Al) of the P2 position was calculated as 1.59, corresponding to a transition phase of Ht and saponite. The thicknesses of the transition areas were usually less than those of the core and the shell regions, implying that the transformation of hydrotalcite to saponite was a dissolution-recrystallization process. This process proceeded further with the extension of reaction times, and almost all the Ht could be converted to saponite when the required cations were at an appropriate concentration ratio.

Hydrothermal Transformation mechanism

To confirm the proposition that that saponite arose by transformation of Ht, we reacted Ht with different Mg/Al ratios along with SiO_3^{2-} under hydrothermal conditions. The as-synthesized Ht was well crystallized and without any impurities. The reflections in the region of 10.85–9.93° (2θ), corresponding to d_{003} values of 0.800–0.880 nm (Fig. 8) are larger than the pure carbonate anion intercalated Ht. This observation may be ascribed to the incorporation of some NO_3^- along with CO_3^{2-} during the co-precipitation process (Duan and Evans, 2006).

After four days of hydrothermal reaction, all the Ht reflections decreased sharply

in intensity. Meanwhile, a series of new reflections corresponding to (001), (02, 11), (13, 20) and (060) of saponite intensified. Among them, the d_{001} reflections were in the range of 1.36–1.53 nm and the d_{060} was at about 0.154 nm, confirming the formation of a typical tri-octahedral smectite, *i.e.,* saponite. The products contained analcite and gibbsite as impurities, indicative of an enriched Si and Al environment. As the Mg/Al ratio increased, these impurities decreased (Fig. 8). Thus, the present results clearly suggest the transformation of Ht to saponite, a 2:1 type clay under a silicate-rich alkaline condition.

Based upon the above results, it was concluded that the whole transformation process was through a rehydration-dissolution-precipitation pathway (Fig. 9). The transformation process started with the construction of hydrotalcite from metal oxides, followed by partial dissolution of Al^{3+} from Ht and subsequent condensation of metasilicate anions with Ht, and ended with crystallization of saponite. The process was preconditioned by the coexistence of and the condensation among silicate anions, and was greatly accelerated by the substitution of Si^{4+} by Al^{3+} in silicate oligomers, the Al^{3+} ions being dissolved from hydrotalcite. The substitution of Al^{3+} resulted in the generation of negatively charged tetrahedral sheets. This study shows for the first time that CO_2 is an indispensable component during the transformation processes. This compound is intercalated as CO_3^{2-}, giving rise to Ht, and expelled allowing Mg-smectite to form.

This is a preprint, the final version is subject to change, of the American Mineralogist (MSA)
Cite as Authors (Year) Title. American Mineralogist, in press.
DOI: https://doi.org/10.2138/am-2019-7043

IMPLICATIONS

The rare occurrence of hydrotalcite on the Earth is a long-standing unsolved puzzle. Coincidentally, a similar situation also exists on the Martian surface, where the distribution of carbonate deposits is very limited and isolated, in contrast to the abundant and widespread Mg-smectite deposits (Ehlmann and Edwards, 2014; Peretyazhko *et al.*, 2018; Wray, 2016;). Our study shows that Ht may form and subsequently transform to saponite directly during hydrothermal alteration of basalt-like solids under alkaline conditions. Saponite is often found with carbonates under high pH and silicate and/or Mg-rich conditions (eg. alkaline lakes and evaporative basins) (Milesi *et al.*, 2018; Polyak *et al.*, 2000). To the best of our knowledge, however, the direct conversion of carbonates to saponite, and the factors influencing the process, have not been previously investigated. This transformation provides one possible explanation for the rarity of the natural Ht deposits or the other carbonate minerals with similar chemical stabilities on the surface of the Earth (or even the surface of Mars).

The aforementioned transformation is mediated by a hydration-dissolution-precipitation pathway. The process depended on factors such as dissolution of Al^{3+} from Ht and isomorphous substitution of Al^{3+} for Si^{4+} in silicate oligomers. The resultant negatively charged oligomers then condense with Ht to form TOT layers of saponite. Condensation is also favored by the low Mg/Al ratios and the

high concentrations of $Al^{3+}$and silicate oligomers**,** and resulted in saponite of much higher crystallinity. The formation of saponite from metal oxides, via hydrotalcite, under hydrothermal conditions provides insight into the chemical stability of the different mineral phases as well as into metal availability in soils (Jacquat *et al*., 2008; 2009).

We further propose that CO_2 is an indispensable component in the process. Initially intercalated as CO_3^{2-} to form Ht, CO_2 is subsequently released from the solid phase, and saponite is formed when the layer charge is reversed. This may also have implications for the carbon cycle on the surface of the Earth.

ACKOWLEDGEMENT

This work was financially supported by National Natural Science Foundation of China (grant numbers 41772039 and 41530313), CAS Key Research Program of Frontier Sciences (grant number QYZDJSSW-DQC023-1), and Guangdong Provincial Youth Top-notch Talent Support Program (grant number 2015TQ01Z797). One of us (SK) was supported by the College of Agricultural Sciences under Station Research Project No. PEN04566. We are grateful to Dr. Hexiong Yang, The University of Arizona, and the reviewers for constructive comments and suggestions.

ENDNOTE

Supplementary Information associated with this article can be found, in the online

467 version.

468

469 ## REFERENCES CITED

470 Abdelouas, A., Crovisier, J.L., Lutze, W., Fritz, B., Mosser, A. and Mueller, R.
471 (1994) Formation of hydrotalcite-like compounds during R7T7 nuclear waste glass and
472 basaltic glass alteration. Clays and Clay Minerals, 42, 526-533.

473 Allen, C.C., Gooding, J.L., Jercinovic, M., Keil, K. (1981) Altered basaltic glass:
474 A terrestrial analog to the soil of Mars. Icarus, 45, 347-369.

475 Auerbach, S.M., Carrado, K.A., Dutta, P.K. (2004) Handbook of Layered
476 Materials. New York: Marcel Dekker.

477 Baskaran, T., Kumaravel, R., Christopher, J. and Sakthivel, A. (2013) Silicate
478 anion-stabilized layered magnesium-aluminium hydrotalcite, RSC Advances, 3,
479 16392-16398.

480 Bisio, C., Gatti, G., Boccaleri, E., Marchese, L., Superti, G., Pastore, H.O. and
481 Thommes, M. (2008) Understanding physico-chemical properties of saponite synthetic
482 clays, Microporous and Mesoporous Materials, 107, 90-101.

483 Botha, G.A., Hughes, J.C. (1992) Pedogenic palygorskite and dolomite in a Late
484 Neogene sedimentary succession, northwestern Transvaal, South Africa, Geoderma, 53,
485 139-154.

Dehouck, E., Gaudin, A., Mangold, N., Lajaunie, L., Dauzères, A., Grauby, O., and Le Menn, E. (2014) Weathering of olivine under CO_2 atmosphere: A Martian perspective, Geochimica et Cosmochimica Acta, 135, 170-189.

Duan, X., and Evans, D.G. (2006) Layered Double Hydroxides. Berlin, Heidelberg: Springer.

Ehlmann, B.L., and Edwards, C.S. (2014) Mineralogy of the Martian Surface, Annual Review of Earth and Planetary Sciences, 42, 291-315.

Farmer, V. C. (1974) The infrared spectra of minerals, Monograph, London: Mineralogical Society.

Fyfe, C.A., Fu, G., and Grondey, H. (1994) Pillaring of layered double hydroxides with cage-like polysilicates: A possible new class of base catalysts or catalyst precursors. Pittsburgh: Materials Research Society.

Golden, D.C., Ming, D.W., Morris, R.V., and Mertzman, S.A. (2005) Laboratory-simulated acid-sulfate weathering of basaltic materials: Implications for formation of sulfates at Meridiani Planum and Gusev crater, Mars, Journal of Geophysical Research: Planets 110, 1-15.

Gooding, J. L., and Keil, K. (2013) Alteration of glass as a possible source of clay minerals on Mars, Geophysical Research Letters, 5, 727-730.

He, H.P., Li, T., Tao, Q., Chen, T.H., Zhang, D., Zhu, J.X., Yuan, P., and Zhu, R.L.

505 (2014) Aluminum ion occupancy in the structure of synthetic saponites: Effect on
506 crystallinity, American Mineralogist, 99, 109-116.

507 Huang, J., Chu, X., Lyons, T.W., Planavsky, N.J. and Wen, H. (2013) A new look
508 at saponite formation and its implications for early animal records in the Ediacaran of
509 South China. Geobiology, 11, 3–14.

510 Ishihara, S., Sahoo, P., Deguchi, K., Ohki, S., Tansho, M., Shimizu, T., Labuta, J.,
511 Hill, J.P., Ariga, K., Watanabe, K., Yamauchi, Y., Suehara, S., Iyi, N. (2013) Dynamic
512 breathing of CO_2 by hydrotalcite, Journal of the American Chemical Society, 135(48),
513 18040-18043

514 Jacquat, O., Voegelin, A., Kretzschmar, R. (2009) Soil properties controlling Zn
515 speciation and fractionation in contaminated soils. Geochimica et Cosmochimica Acta,
516 73, 5256-5272.

517 Jacquat, O., Voegelin, A., Villard, A., Marcus, M.A., Kretzschmar, R. (2008)
518 Formation of Zn-rich phyllosilicate, Zn-layered double hydroxide and hydrozincite in
519 contaminated calcareous soils. Geochimica et Cosmochimica Acta, 72, 5037-5054.

520 Kahle, C. (1965) Possible roles of clay minerals in the formation of dolomite.
521 Journal of Sedimentary Research, 35, 448-453.

522 Lipsicas, M., Raythatha, R.H., Pinnavaia, T.J., Johnson, I.D., Giese, Jr. R.F.,
523 Costanzo, P. M., and Robert, J.-L. (1984) Silicon and aluminium site distributions in

524 2:1 layered silicate clays. Nature, 309, 604-607.

525 Liu, D., Xu, Y., Papineau, D., Yu, N., Fan, Q., Qiu, X., Wang, H. (2019)
526 Experimental evidence for abiotic formation of low-temperature proto-dolomite
527 facilitated by clay minerals. Geochimica et Cosmochimica Acta, 247, 83-95.

528 Martín-Pérez, A., Alonso-Zarza, A.M., Iglesia, A.L., Martín-García, R. (2015) Do
529 magnesian clays play a role in dolomite formation in alkaline environments? An
530 example from Castañar Cave, Cáceres (Spain), Geogaceta, 57, 15-18.

531 Milesi, V.P., Jezequel, D., Debure, M., Marty, N., Guyot, F.J., Claret, F., Virgone,
532 A., Gaucher, E., and Ader, M. (2018) Formation of Mg-aluminosilicates during early
533 diagenesis of carbonate sediments in the volcanic crater lake of Dziani Dzaha (Mayotte
534 - Indian Ocean). Sedimentology, Doi: 10.1111/sed.12531.

535 Peretyazhko, T.S., Niles, P.B., Sutter, B., Morris, R.V., Agresti, D.G., Le, L., and
536 Ming, D.W. (2018) Smectite formation in the presence of sulfuric acid: Implications for
537 acidic smectite formation on early Mars, Geochimica et Cosmochimica Acta, 220,
538 248-260.

539 Polyak, V.J. and Güven, N. (2000) Authigenesis of trioctahedral smectite in m
540 agnesium –rich carbonate speleothems in Carlsbad cavern and other caves of the
541 Guadalupe Mountains, New Mexico, Clays and Clay Minerals, 48, 317-321.

542 Schutz, A., and Biloen, P. (1987) Interlamellar chemistry of hydrotalcites: I.

543 Polymerization of silicate anions, Journal of Solid State Chemistry, 68, 360-368.

544 Setti, M., Marinoni, L. and Lopez-Galindo, A. (2004) Mineralogical and
545 geochemical characteristics (major, minor, trace elements and REE) of detrital and
546 authigenic clay minerals in a Cenozoic sequence from Ross Sea, Antarctica. Clay
547 Minerals, 39, 405–421.

548 Shao H., and Pinnavaia T.J. (2010) Synthesis and properties of nanoparticle forms
549 saponite clay, cancrinite zeolite and phase mixtures thereof, Microporous and
550 Mesoporous Materials, 133, 10-17.

551 Smith K.A., Kirkpatrick R.J., Oldfield E., and Henderson D.M. (1983)
552 High-resolution Si-29 nuclear magnetic-resonance spectroscopic study of
553 rock-forming silicates, American Mineralogist, 68, 1206-1215.

554 Tao, Q., Chen, M.Y., He, H.P., and Komarneni, S. (2018) Hydrothermal
555 transformation of mixed metal oxides and silicate anions to phyllosilicate under highly
556 alkaline conditions, Applied Clay Science, 156, 224-230.

557 Tao, Q., Fang, Y., Li, T., Zhang, D., Chen, M.Y., Ji, S.C, He, H.P., Komarneni, S.,
558 Zhang, H.B., Dong, Y., Noh, Y.D. (2016) Silylation of saponite with
559 3-aminopropyltriethoxysilane, Applied Clay Science, 132-133, 133-139.

560 Tao, Q., Zhu, J.X., Wellard, R.M., Bostrom, T. E., Frost, RL., Yuan, P., and He, H.P.
561 (2011) Silylation of layered double hydroxides via an induced hydrolysis method,

562 Journal of Materials Chemistry, 21, 10711-10719.

563 Tao, Q., Zhu, J.X., Frost, R.L., Bostrom, T.E., Wellard, R.M., Wei, J.M., Yuan, P.,
564 and He, H.P. (2010) Silylation of layered double hydroxides via a
565 calcination-rehydration route, Langmuir, 26, 2769-2773.

566 Tosca, N. J. (2015) Geochemical pathways to Mg-clay formation. In: Magnesian
567 Clays: Characterization, origins and applications (Eds M. Pozo and E. Galán). AIPEA
568 Special Publications, 2, 283–329.

569 Tosca, N. J., Miliken, R. E., and Michel, F. M. (2008) Smectite Formation on Early
570 Mars: Experimental Constraints, Workshop on Martian Phyllosilicates: Recorders of
571 Aqueous Processes, Pairs, No. 1441, 77-78.

572 Vogels, R.J.M.J., Kloprogge, J.T., and Geus, J.W. (2005) Synthesis and
573 characterization of saponite clays, American Mineralogist, 90, 931-944.

574 Wray, J. J., Murchie, S. L., Bishop, J. L., Ehlmann, B. L., Milliken, R. E., Wilhelm,
575 M. B., Seelos, K. D., and Chojnacki, M. (2016) Orbital evidence for more widespread
576 carbonate-bearing rocks on Mars, Journal of Geophysical Research: Planets, 121,
577 652–677.

578 Wanas, H.A., Sallam, E. (2016) Abiotically-formed, primary dolomite in the
579 mid-Eocene lacustrine succession at Gebel El-Goza El-Hamra, NE Egypt: an approach
580 to the role of smectitic clays, Sedimentary Geology, 343, 132-140.

581 Yun, S.K. (1995) Synthesis and catalytic properties of silicate-intercalated layered
582 double hydroxides formed by intragallery hydrolysis of tetraethylorthosilicate, Clays
583 and Clay Minerals, 43, 503-510.

584 Zeyen, N., Daval, D., Lopez-Garcia, P., Moreira, D., Gaillardet, J. and Benzerara,
585 K. (2017) Geochemical conditions allowing the formation of modern lacustrine
586 microbialites. Procedia Earth Planetary Science, 17, 380-383.

587

This is a preprint, the final version is subject to change, of the American Mineralogist (MSA)
Cite as Authors (Year) Title. American Mineralogist, in press.
DOI: https://doi.org/10.2138/am-2019-7043

588

TABLES

Table 1. XRF analyses of MMOs and their hydrothermal products synthesized using different reaction times.

Sample	SiO_2 ($_{wt}$%)	Al_2O_3 ($_{wt}$%)	MgO ($_{wt}$%)	Na_2O ($_{wt}$%)	L.O.I ($_{wt}$%)	Total ($_{wt}$%)	Mg/Al[#]	Si/Al[#]
MMO-2	—	32.42	60.43	0.53	5.66	99.99	2.38	—
MMO-2-0	3.08	24.12	46.52	0.40	24.30	99.89	2.46	0.11
MMO-2-1	31.48	15.44	27.47	5.85	18.57	99.74	2.27	1.73
MMO-2-4	39.09	13.96	24.72	7.26	13.70	99.54	2.26	2.38
MMO-2-10	41.83	14.02	25.30	7.41	10.43	99.79	2.30	2.54
MMO-2-15	41.17	14.05	24.62	7.71	11.17	99.52	2.24	2.49
MMO-4	—	19.71	73.51	0.95	3.81	99.36	4.76	—
MMO-4-0	2.68	13.09	49.64	0.17	33.01	100.08	4.83	0.17
MMO-4-1	34.63	9.60	34.17	2.95	17.44	99.74	4.54	3.06
MMO-4-4	39.34	9.25	32.75	3.21	14.35	99.80	4.51	3.61
MMO-4-10	42.41	8.96	31.48	3.65	12.60	99.94	4.48	4.02
MMO-4-15	43.00	9.00	31.24	3.77	12.12	99.96	4.43	4.06
MMO-6	—	13.85	79.54	0.51	4.47	99.71	7.32	—
MMO-6-0	3.56	9.15	54.19	0.21	31.34	99.97	7.55	0.33
MMO-6-1	23.71	7.39	41.27	0.97	25.33	99.91	7.12	2.73
MMO-6-4	30.77	6.93	37.79	1.96	21.53	100.01	6.95	3.77
MMO-6-10	34.51	6.82	36.16	2.32	18.98	99.77	6.76	4.30
MMO-6-15	45.25	6.23	32.40	3.01	11.82	99.52	6.63	6.17

[#] Mole ratio. — N.A.

589

590 # FIGURE CAPTIONS

591 FIGURE 1. XRD patterns of MMO and their hydrothermally treated products
592 (series A: MMO-2, series B: MMO-4 and series C: MMO-6). a. MMO-n, b. MMO-n-0,
593 c. MMO-n-1, d. MMO-n-4, e. MMO-n-10, f. MMO-n-15, g. MMO-n-30, and h.
594 MMO-n-60.

595 FIGURE 2. ^{27}Al (left) and ^{29}Si (right) NMR spectra of MMO with different Mg/Al
596 ratios and their hydrothermal products. a. MMO-2, b. MMO-4, c. MMO-6, d.
597 MMO-2-4, e. MMO-4-4, f. MMO-6-4, g. MMO-2-15, h. MMO-4-15, and i.
598 MMO-6-15.

599 FIGURE 3. XRD patterns of MMO-4 hydrothermal products formed with
600 different SiO_3^{2-} concentrations. a. MMO-4-4-0.5AEC, b. MMO-4-15-0.5AEC, c.
601 MMO-4-4-1.0AEC, d. MMO-4-15-1.0AEC. e. MMO-4-4-4.0AEC, f.
602 MMO-4-15-4.0AEC, g. MMO-4-4, and h. MMO-4-15.

603 FIGURE 4. ^{27}Al (left) and ^{29}Si (right) NMR spectra of MMO-4 hydrothermal
604 products formed with different SiO_3^{2-} concentrations. a. MMO-4-4-0.5AEC, b.
605 MMO-4-15-0.5AEC, c. MMO-4-4-1.0AEC, d. MMO-4-15-1.0AEC, e.
606 MMO-4-4-4.0AEC, f. MMO-4-15-4.0AEC, g. MMO-4-4-11AEC, and h.
607 MMO-4-15-11AEC.

608 FIGURE 5. TEM images and EDS results of MMO-2-1. a. long columnar

609 natrodavyne and lamellar saponite; b. lamellar saponite, c. natrodavyne and its EDS
610 results (P1), and d. saponite and its EDS results (P2).

611 FIGURE 6. TEM images and SEAD patterns of MMO-6-2. a. morphology of
612 crystal aggregates, b. morphology of a single particle, P1–P3 represent the SEAD
613 patterns of the selected position in the single particle (b).

614 FIGURE 7. TEM images (up) and SEAD patterns (down) of MMO-6-4. P1–P3
615 represent the SEAD patterns and their EDS results of the selected position in the single
616 particle.

617 FIGURE 8. XRD patterns of Ht samples with different Mg/Al ratios and their
618 hydrothermal products after incorporation of SiO_3^{2-}. a. Ht-2, b. Ht-4, c. Ht-6, d. Ht-2-4,
619 e. Ht-4-4, f. Ht-6-4.

620 FIGURE 9. Schematic of the formation of smectite from metal oxides via
621 hydrotalcite.

622

This is a preprint, the final version is subject to change, of the American Mineralogist (MSA)
Cite as Authors (Year) Title. American Mineralogist, in press.
DOI: https://doi.org/10.2138/am-2019-7043

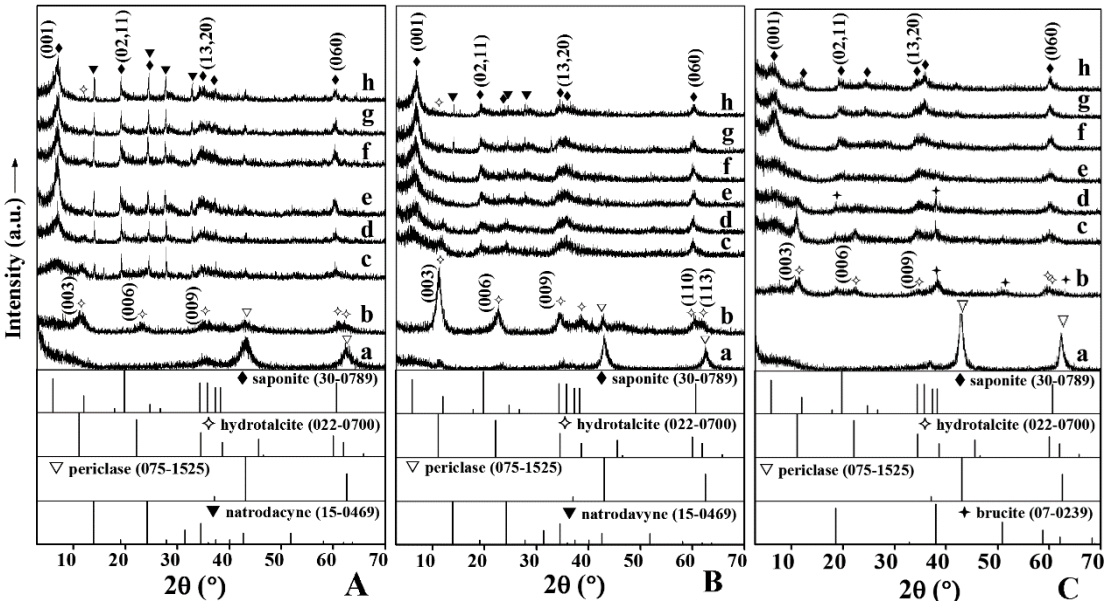

623

624 **Figure 1**

625

This is a preprint, the final version is subject to change, of the American Mineralogist (MSA)
Cite as Authors (Year) Title. American Mineralogist, in press.
DOI: https://doi.org/10.2138/am-2019-7043

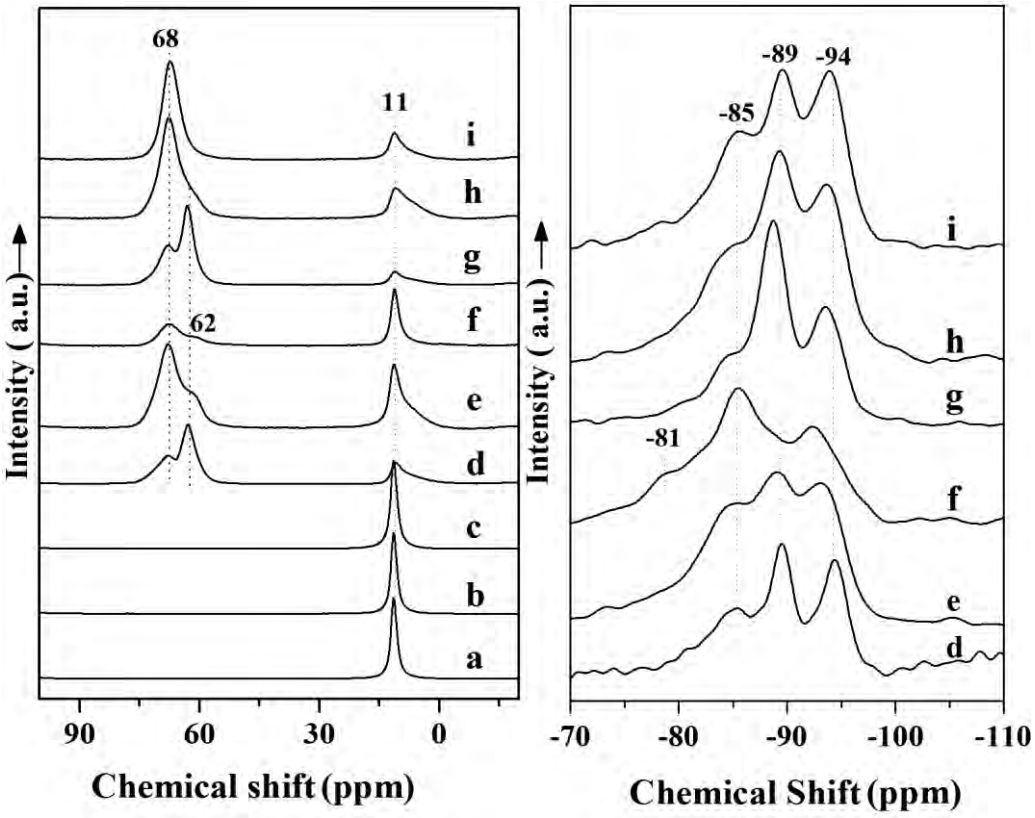

626

627 **Figure2**

628

This is a preprint, the final version is subject to change, of the American Mineralogist (MSA)
Cite as Authors (Year) Title. American Mineralogist, in press.
DOI: https://doi.org/10.2138/am-2019-7043

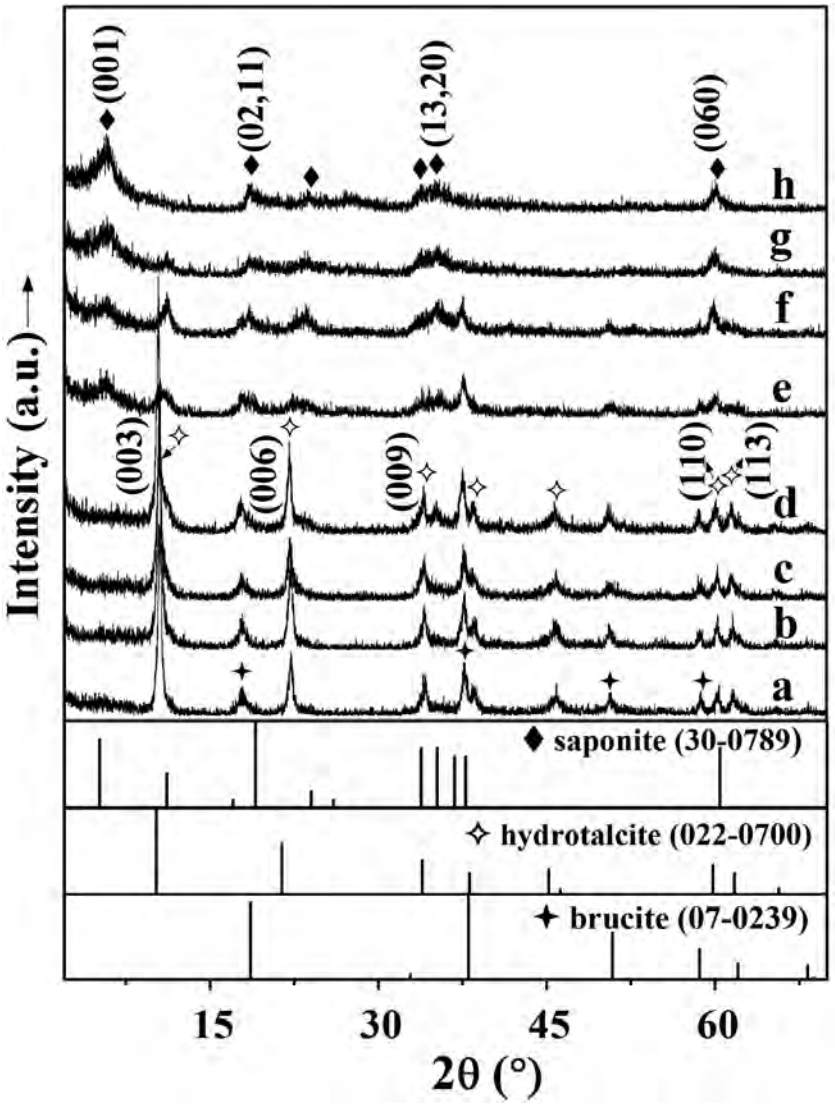

629

630 **Figure 3**

631

This is a preprint, the final version is subject to change, of the American Mineralogist (MSA)
Cite as Authors (Year) Title. American Mineralogist, in press.
DOI: https://doi.org/10.2138/am-2019-7043

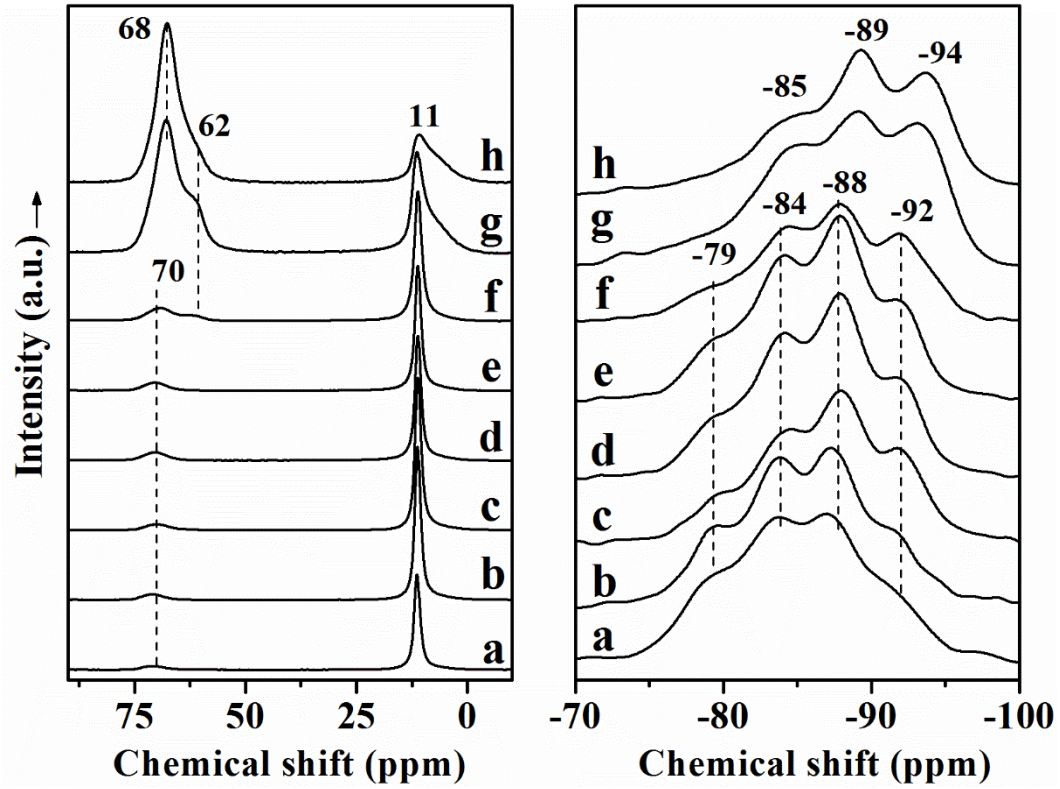

632

633 **Figure 4**

634

This is a preprint, the final version is subject to change, of the American Mineralogist (MSA)
Cite as Authors (Year) Title. American Mineralogist, in press.
DOI: https://doi.org/10.2138/am-2019-7043

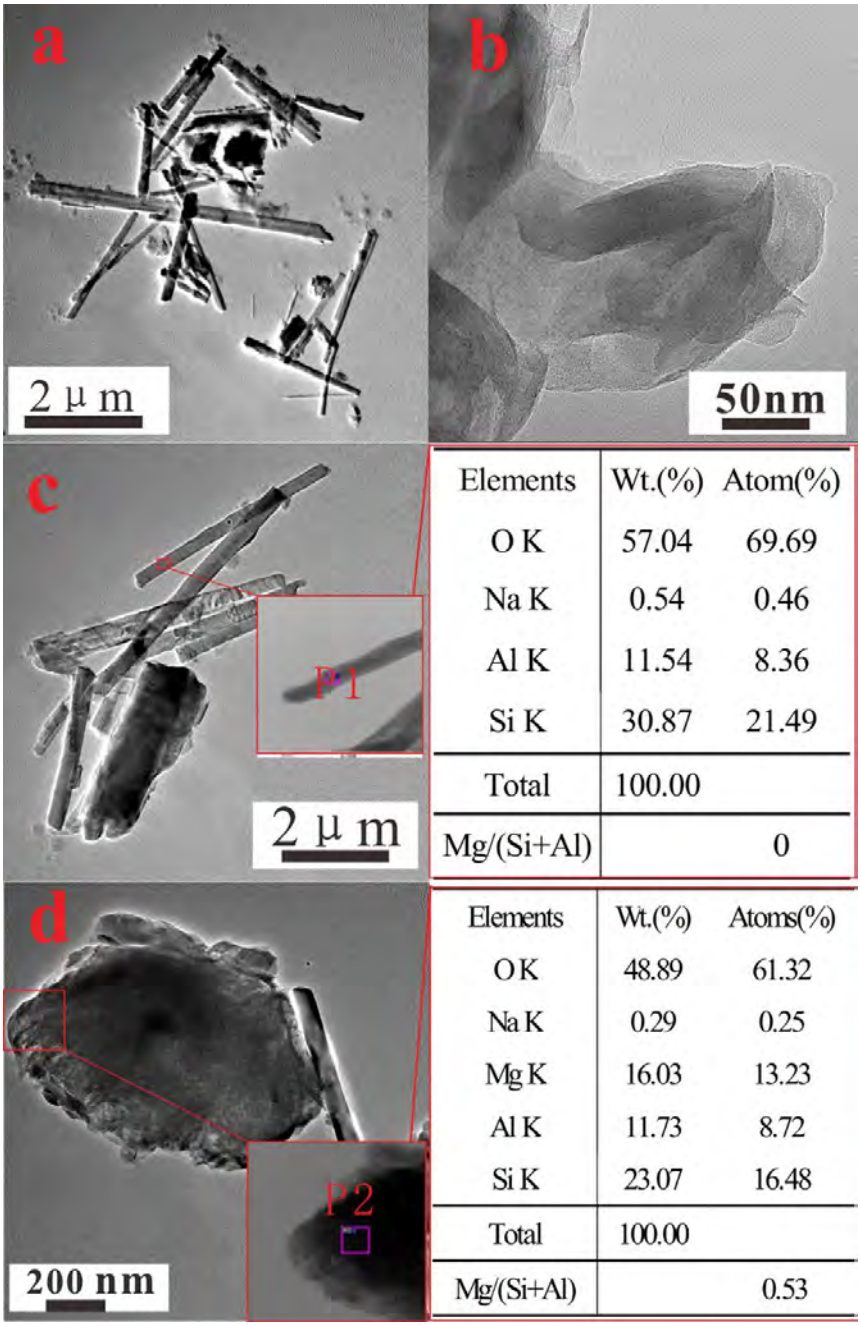

Elements	Wt.(%)	Atom(%)
O K	57.04	69.69
Na K	0.54	0.46
Al K	11.54	8.36
Si K	30.87	21.49
Total	100.00	
Mg/(Si+Al)		0

Elements	Wt.(%)	Atoms(%)
O K	48.89	61.32
Na K	0.29	0.25
Mg K	16.03	13.23
Al K	11.73	8.72
Si K	23.07	16.48
Total	100.00	
Mg/(Si+Al)		0.53

635

636 **Figure 5**

637

This is a preprint, the final version is subject to change, of the American Mineralogist (MSA)
Cite as Authors (Year) Title. American Mineralogist, in press.
DOI: https://doi.org/10.2138/am-2019-7043

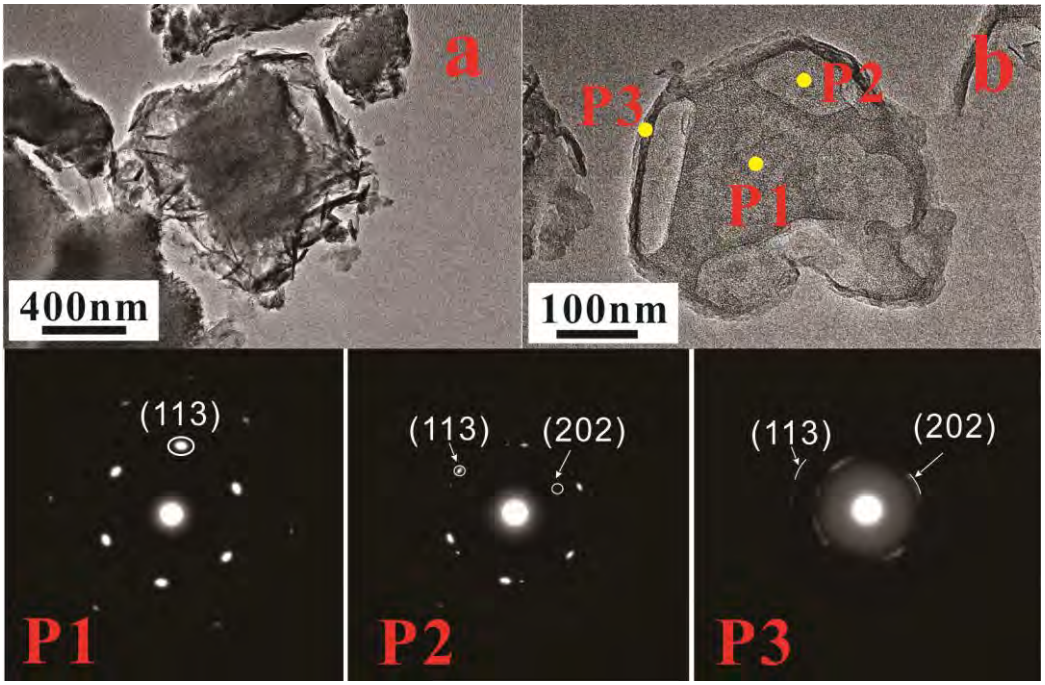

638

639 **Figure 6**

640

This is a preprint, the final version is subject to change, of the American Mineralogist (MSA)
Cite as Authors (Year) Title. American Mineralogist, in press.
DOI: https://doi.org/10.2138/am-2019-7043

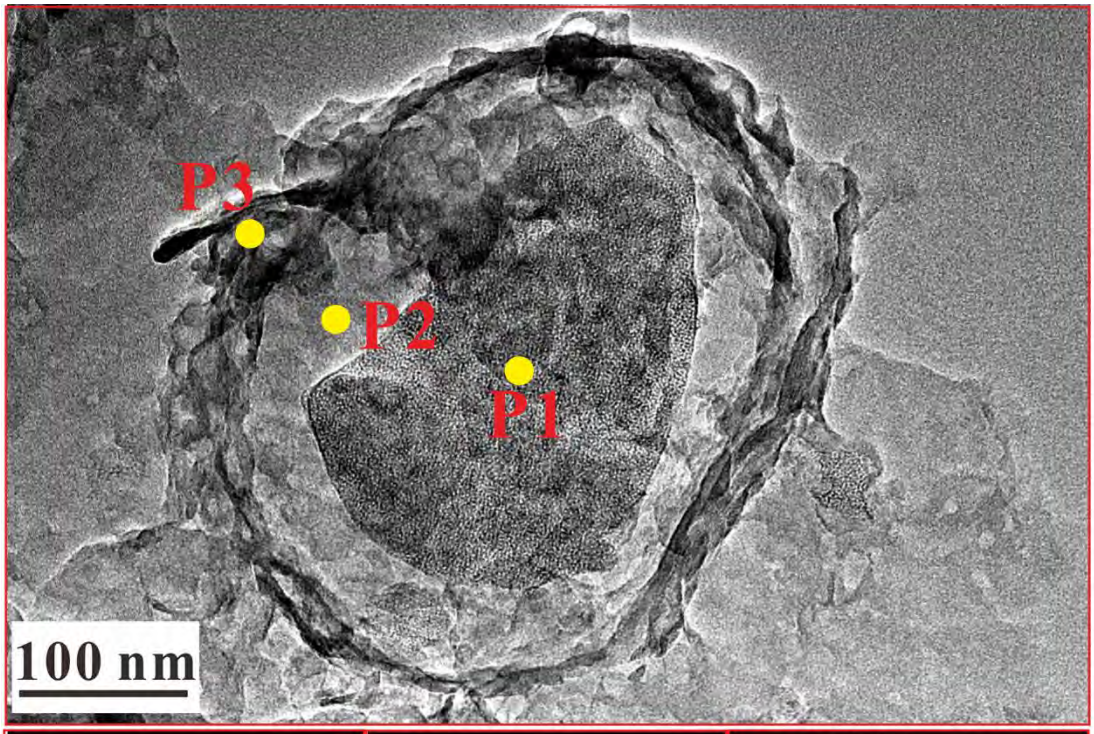

Elements	Wt.(%)	Atom(%)
C K	7.36	11.68
O K	40.30	48.01
Na K	0.24	0.20
Mg K	44.02	34.51
Al K	4.23	2.99
Si K	3.85	2.62
Total	100.00	
Mg/(Si+Al)		6.15

Elements	Wt.(%)	Atom(%)
C K	9.18	14.57
O K	39.87	47.49
Na K	-0.20	-0.17
Mg K	29.84	23.39
Al K	9.12	6.44
Si K	12.20	8.28
Total	100.00	
Mg/(Si+Al)		1.59

Elements	Wt.(%)	Atom(%)
C K	4.31	7.13
O K	43.17	53.58
Na K	-0.11	-0.09
Mg K	18.11	14.79
Al K	6.36	4.68
Si K	28.15	19.91
Total	100.00	
Mg/(Si+Al)		0.61

641

642 **Figure 7**

643

This is a preprint, the final version is subject to change, of the American Mineralogist (MSA)
Cite as Authors (Year) Title. American Mineralogist, in press.
DOI: https://doi.org/10.2138/am-2019-7043

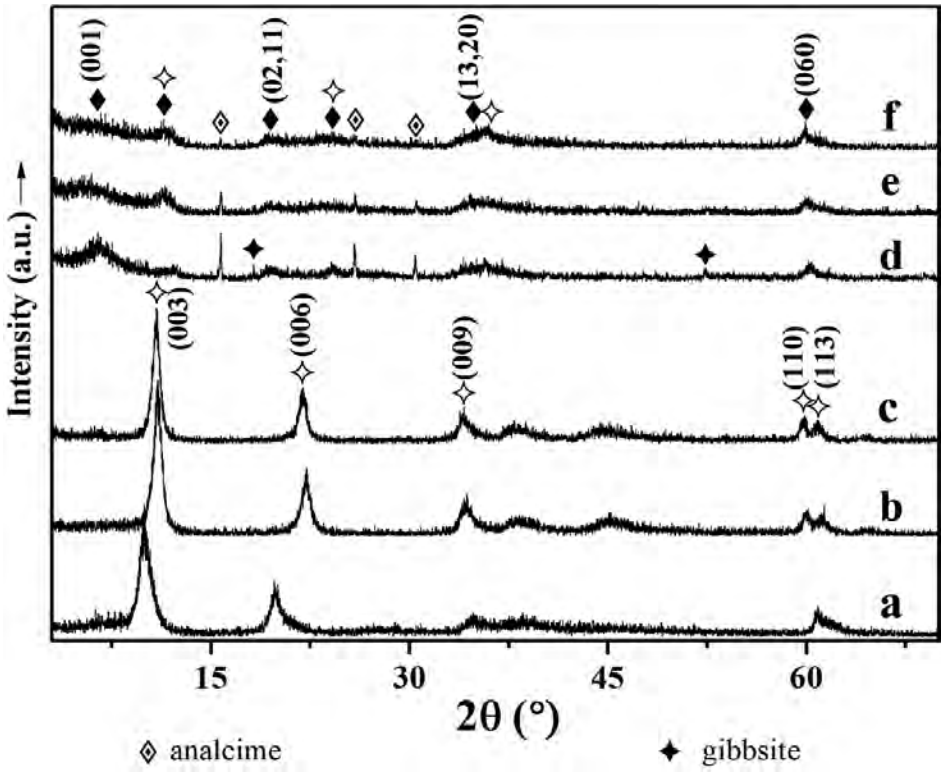

644

645 **Figure 8**

646

This is a preprint, the final version is subject to change, of the American Mineralogist (MSA)
Cite as Authors (Year) Title. American Mineralogist, in press.
DOI: https://doi.org/10.2138/am-2019-7043

647

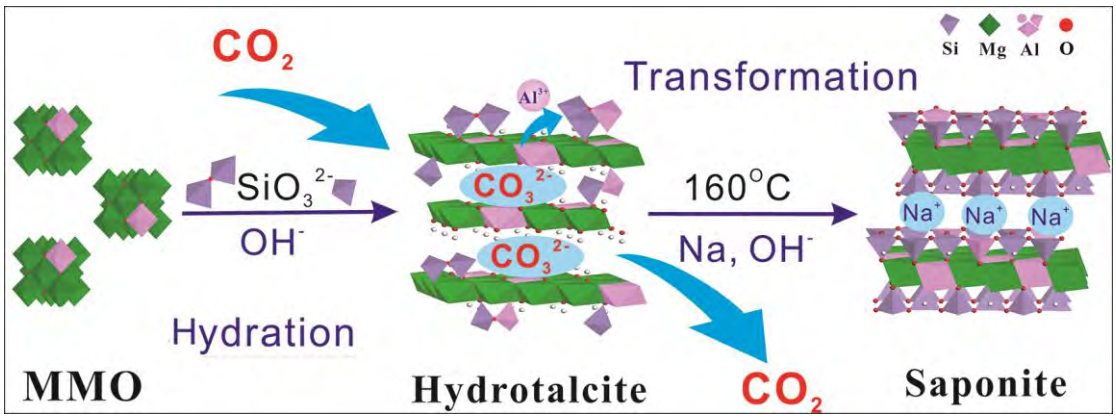

648

649 **Figure 9**

650